International Journal of Adhesion & Adhesives 112 (2022) 103024

Contents lists available at ScienceDirect

International Journal of Adhesion and Adhesives

journal homepage: www.elsevier.com/locate/ijadhadh

Using contact angle measurement technique for determination of the surface free energy of B-SBA-15-x materials

Alime Çıtak [a,*], Tuğba Yarbaş [b]

[a] Chemical Engineering Department, Eskişehir Osmangazi University, 26480, Eskişehir, Turkey
[b] Information Technology Department, Bilecik Seyh Edebali University, 11230, Bilecik, Turkey

ARTICLE INFO

Keywords:
Surface energy
Contact angle measurement
Boron
B-SBA-15
Direct hydrothermal synthesis
Mesoporous materials

ABSTRACT

Pure and boron-containing, Santa Barbara Amorphous (SBA-15) mesoporous materials and B-SBA-15-x (x is molar ratio of Si/B = 50, 30, 10), were synthesized via a direct hydrothermal method. Samples were characterized by XRD, BJH pore size distribution and SEM techniques. A contact angle technique was used to determine surface free energy and its dispersive and polar components. For this purpose, ethylene glycol (EG), diiodomethane (DIM), formamide (FA) and water were used as model liquids to detect the contact angles. The OWRK/Fowkes approach was used to calculate the surface free energy values. Total surface free energy (γ_S) values of pure SBA-15 and B-SBA-15-50, B-SBA-15-30, B-SBA-15-10 were calculated as 64.365, 63.545, 63.490 and 64.218 mJ/m^2 at room temperature, respectively. The main results of the study can be summarized as follows: (*i*) The contact angle measurement technique is suitable for determining the total surface free energy (γ_S) and its dispersive and polar components (γ_S^d and γ_S^p, respectively) of SBA-15 mesoporous materials and (*ii*) Addition of boron did not have a significant impact on the characteristic structure of SBA-15.

1. Introduction

The contact angle formed by solid and liquid substances is an important parameter in industrial products such as adhesives, coatings, paints, cosmetics and some medical devices, and the surface free energy (SFE) of solids can be calculated using contact angle values [1]. The surface free energy of a powder material has an important role in determining physicochemical properties such as wettability, adhesion, and flowability. Also both surface wettability and surface free energy are affected by physical and chemical changes of the solid surface [2].

Contact angle measurement is one of the most commonly used techniques for solid surface characterization [3]. In contact angle measurements, image analysis is performed and this method is a reliable method that ensures the accuracy and repeatability of test results [4]. The contact angle is formed by the liquid in contact with the surface of different solids and helps to understand the surface properties of the solid. For this purpose, the "sessile drop method" is often used to measure the contact angle [1,2,5–7]. The surface free energy of the solid is rather calculated from the Young equation on the basis of the contact angle for model liquids [8]. There are several approaches such as the Zisman [9], Fowkes [10], Owens–Wendt–Rabel–Kaelble (OWRK) [11,12], van Oss–Chaudhury–Good [13] and Wu [14] for calculating the surface free energy from equilibrium liquid contact angles.

Nowadays there is increasing interest in new materials with high adsorption capacity because of their usage in industry. Therefore, SBA-15, Mobil Composition of Matter (MCM-41) and zeolite type materials have attracted great attention due to desirable properties such as high surface area, large pore volume and facile functionalization [15]. Compared to other mesoporous materials, SBA-15 stands out with larger pore sizes, hydrothermal stability and a thicker wall structure.

In order to increase the catalytic activity of SBA-15, different methods of loading metals such as Al, Fe, Cr, Co, Mn etc. [16–18] is frequently encountered in the literature. In this way, functional groups are formed on the surface of the support material. Due to its adsorption, refractory and high conductivity properties, boron is a cost-effective mineral used in many fields of industry. It is also known that boron containing materials exhibit enhanced properties such as super hardness, insulation and nonlinear optical behavior [19]. Additionally, some sources have shown that boron-containing catalysts reduce carbon formation and accumulation [20–22]. In addition, the number of boron loaded SBA-15 studies in the literature is less than the others.

Mesoporous SBA-15 is an increasingly important material with its

* Corresponding author.
E-mail address: acitak@ogu.edu.tr (A. Çıtak).

https://doi.org/10.1016/j.ijadhadh.2021.103024

Available online 7 October 2021

high surface area and thermal resistance. Boron is used in many areas of industry due to its adsorption, refractory and high conductivity properties and its minerals are cost-effective. There are a small number of studies on the preparation of boron containing SBA-15 catalysts in the literature. Moreover, the characterization of B-SBA-15 materials by contact angle technique has not been found in the literature.

For this reason, pure and boron loaded SBA-15 samples were synthesized by a direct hydrothermal method, characterized with x-ray diffraction (XRD), BJH (Barrett, Joyner ve Halenda method) pore size distribution and scanning electron microscopy (SEM) and their surface free energy values (γ_S, γ_S^d and γ_S^p) and surface properties were determined via a contact angle measurement technique according to the OWRK/Fowkes approach.

2. Materials and methods

2.1. Catalyst preparation

Pure SBA-15 was synthesized by a hydrothermal procedure. According to typical synthesis of SBA-15 [23,24], pluronic 123 triblock copolymer (Aldrich) and TEOS (Aldrich) were used as surfactant and silica source, respectively. 2.005 g P123 was dissolved in water. 60.75 g of aqueous 2 M HCl was added to the solution and then 4.27 g of TEOS was added drop by drop. The mixture was stirred at 35 °C for 20h, transferred to an autoclave and aged at 100 °C for 24 h. The product was filtered, washed, dried and calcined at 540 °C with dry air for 6h with a heating rate of 1°Cmin^{-1}. B-SBA-15-x samples were synthesized also by a direct hydrothermal procedure [17]. The only difference from pure SBA-15 was the addition of calculated amounts of boron after TEOS addition.

2.2. Characterization

XRD patterns were recorded on a Panalytical/Empyrean X-Ray Diffraction instrument operating at 45 kV and 40 mA using Cu Kα radiation ($\lambda = 0.15406$ nm) in the 2θ range of 0–80° with a 2θ step size of 0.02°.

BJH pore size distributions of the samples were measured via N_2 adsorption at −196 °C on a Micromeritics ASAP 2020 apparatus with all samples outgassed at 250 °C for 180 min under vacuum before measurement.

Scanning electron microscopy (SEM) images were obtained with a JEOL JSM-5600 LV microscope (at 20 kV, x7500 zoom and 2 μm for B-SBA-15-x samples, operating conditions).

2.3. Contact angle measurements

Contact angle tests were carried out by dropping model liquids on the pelleted samples with an Attention Theta Lite contact angle measuring device. Sessile drop method was used for determination of the wettability of samples. The synthesized particulate mesoporous materials (samples) were made into pellets by applying 1–2 tons of pressure to obtain a smooth surface. At least 4 pellets were prepared from each sample because of the 4 model liquids. Static contact angles were measured using four model liquids: EG and DIM were used as non-polar model liquids; FA and water were used as polar model liquids. Based on device measurements, the average droplet volumes of each model liquid at first contact with the solid surface were as follows: water, EG, FA and DIM were approximately 9 μl, 10 μl, 10 μl and 3 μl, respectively. Experimental studies were conducted at room temperature.

Using the pellets obtained from the synthesized samples, the contact angles (θ) formed by a single drop of each model liquid were examined and recorded by the software program named "One Attention" on the computer connected to the device. Image records were set to 10 s at % 100FPS. The angle values formed between the determined baseline and the right and left contact points of the model liquid droplet with the solid surface were measured by the program. The program averages the angle values of the right and left points. The final average contact angle after10 s of the experimental period was calculated by averaging of all the mean values. However, some non-significant data at the first contact of the liquid droplet with the solid surface and inconsistent data recorded from time to time were excluded from the mean.

Measurements were taken for each model liquid separately and the final contact angles were determined according to the method described above. The contact angles of model fluids with samples are listed in Table 2.

The OWRK/Fowkes approach was used for surface free energy calculations. The surface free energies of samples and its components are listed in Table 3.

Experiments were repeated when inconsistent results were obtained.

2.4. Surface energy determination model

There are several theoretical models to calculate surface free energy based on contact-angle measurements as mentioned above. In this study, the most commonly used and cited Owens – Wendt – Rabel – Kaelble (OWRK) model [11] was chosen to determine surthe face free energies of samples, also known as the expanded Fowkes model [10] based on the Young – Dupree Equation. This model has been named OWRK/Fowkes by the Attention Theta Lite contact angle device.

Eq (1) shows the Young's Equation:

$$\gamma_L.cos\theta = \gamma_S - \gamma_{SL} \tag{1}$$

where γ_S, γ_L and γ_{SL} are the surface free energies of solid, liquid and solid–liquid (mJ/m^2); θ is the contact angle (°) between solid and liquid, respectively.

γ_L (in Eq (1)) is a characteristic of the model liquid and is known. θ (in Eq (1)) is the contact angle between liquid and solid and can be measured. Therefore, the work of adhesion (W_A) equation is needed to calculate γ_S and γ_{SL} [3]:

$$W_A = \gamma_S + \gamma_L - \gamma_{SL} \tag{2}$$

When Eq (2) is combined with Eq (1):

$$W_A = \gamma_L.(1 + cos\theta) \tag{3}$$

The Owens–Wendt–Rabel–Kaelble (OWRK) model also termed the extended Fowke's model based on the Young–Dupree Equation leads to Eq (4):

$$\gamma_L.(1 + cos\theta) = 2.\left(\sqrt{\gamma_S^d.\gamma_L^d} + \sqrt{\gamma_S^p.\gamma_L^p}\right) \tag{4}$$

where γ_L, γ_L^d and γ_L^p are the total, dispersive and polar surface free energies of liquid and γ_S^d and γ_S^p are the dispersive and polar components of solid surface free energy respectively [3].

3. Results and discussion

3.1. XRD patterns

XRD patterns of the B-SBA-15-x samples are shown in Fig. 1. This indicates that the addition of boron does not lead to a deterioration in the crystal structure of SBA-15 and a uniform SBA-15 structure is formed in all samples. It can be said that the peak seen at approximately 2θ = 22–24° in all B-SBA-15-x samples is the amorphous SiO2 in the structure of SBA-15 [25,26]. Although boron is added to the structure, it is understood that the SBA-15 framework is preserved. On the other hand, the B2O3 phase expected at approximately 2θ = 27–28° was not seen in any sample. This can be explained by the high dispersion of B2O3 particles in

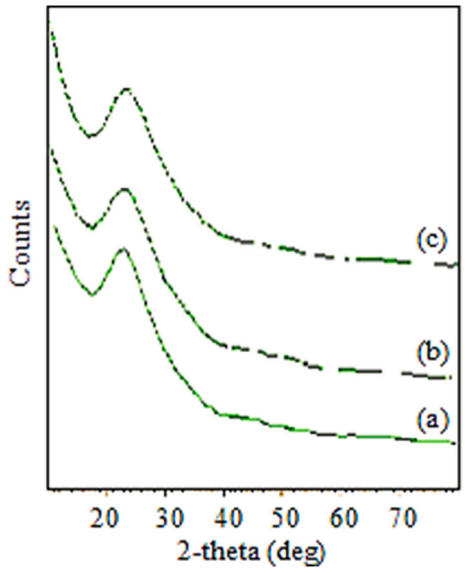

Fig. 1. XRD patterns of B-SBA-15-x samples (a) B-SBA-15-50, (b) B-SBA-15-30 and (c) B-SBA-15-10.

the SBA-15 support and therefore below the XRD detection limit [22]. In a similar situation in the literature, it has been suggested that amorphous glassy boron oxide phases may have been formed due to the difficulty of crystallization of boron oxides [27].

3.2. BJH pore size distributions

Fig. 2 shows BJH pore size distributions of samples. All samples are seen to exhibit uniform pore size distribution and the results seem to be consistent with the literature [28]. Pores between 2 and 50 nm means mesoporous according to the IUPAC classification [29]. In all catalysts it can be said that the pores are mostly in this range. It is understood that the addition of boron does not change the mesoporous structure.

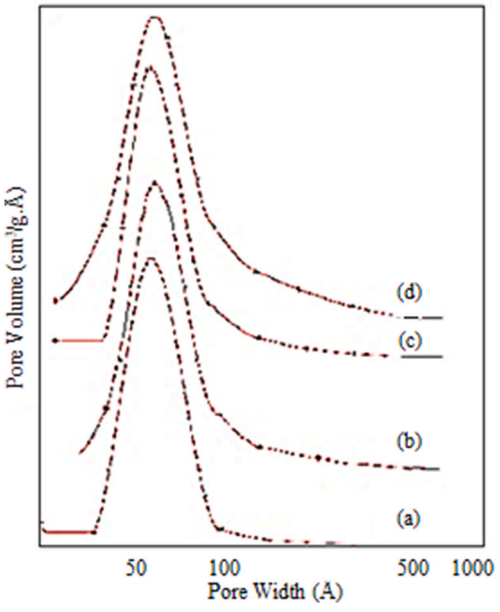

Fig. 2. BJH pore size distributions of (a) pure SBA-15, (b) B-SBA-15-50, (c) B-SBA-15-30 and (d) B-SBA-15-10 samples.

3.3. SEM analyses

Fig. 3 shows SEM images of the B-SBA-15-x samples (for 7500 zoom). Since the amount of boron is low in the B-SBA-15-50 sample, rope-like domains can be seen more clearly than with the other B-SBA-15-x samples. In the B-SBA-15-30 and B-SBA-15-10 samples, although the rope-like areas decreased with increasing boron content, it can still be said to exist.

3.4. Contact angle results

The surface free energy components of model liquids used in the contact angle measurements are given in Table 1.

Contact angles were measured using all model liquids for all samples at room temperature as shown in Table 2. It should be noted here that a smaller contact angle means better wettability of a given solid [33]. Hence a higher contact angle means less adsorption of the model liquid by the sample and thus less interaction between the two. Calculated surface free energy values of the samples according to the OWRK/-Fowkes approach (Eq (4)) at room temperature are given in Table 3.

For EG, the highest contact angle was seen with pure SBA-15 and the lowest contact angle was seen with B-SBA-15-10. Considering the contact angle values, it can be said that increasing the amount of boron in the sample increases the interaction between the sample and EG. Images showing contact angles with EG for all samples can be seen in Fig. 4. Images were taken for 3 different situations which are immediately after dropping (at about time t = 0), shortly after dropping (e.g. 1.97 s as seen in Fig. 4), and approximately at the end of the interaction (at a time when the droplet image in the sample did not change), respectively are compatible with the sample-EG contact angles in Table 2.

The contact angles that DIM formed with the samples could not be correlated with the boron contents of samples. B-SBA-15-30 showed the highest contact angle with DIM (24.653°). The lowest contact angle was seen in pure SBA-15 (18.301°). In other words, the most interacting sample with DIM was pure SBA-15. However, it must be said that the DIM contact angles of the samples are very close to each other, except for B-SBA-15-30. The sample with the most interaction (lowest contact angle) with FA and water was determined as pure SBA-15. In fact, boron oxides are known to be hygroscopic [19]. Therefore, B-SBA-15-x samples could be expected to have higher water adsorption effect than pure SBA-15. However, since the B-SBA-15-x samples were synthesized on the basis of the n_{Si}/n_B molar ratio, the boron contents by weight of samples are actually quite low. Therefore, it can be said that boron species on sample surfaces do not have much effect on wettability.

The lowest contact angles with pure SBA-15 were observed with the polar model liquids (FA and water) (Table 2). There are some results in the literature that show that the polar model liquids (water and formamide) form lower contact angles on surfaces containing more polar groups. In addition, there are results in the literature that show that surface free energy increases with an increase in surface polarity [7]. Considering this situation, it can be interpreted that there are more polar groups on the surface of pure SBA-15 compared to the B-SBA-15-x samples. Again, in accordance with observations in the literature [7], the surface free energy of a sample which had the highest surface polarity was found to be higher than the others in this study (Table 3).

No study has been found in the literature investigating SBA-15 using the contact angle measurement method. Therefore, contact angles of model liquids on SBA-15 samples could not be compared to a similar study in the literature.

Summarizing Table 2, we can say that the lowest contact angles for all model liquids except EG occur with pure SBA-15. So, pure SBA-15 adsorbed DIM, FA and water model liquids more than B-SBA-15-x samples. And this situation generatesexpectation that the surface free energy of pure SBA-15 will be higher than the others. Looking at the total surface free energy(γ_S) in Table 3, it is seen that the surface free energy of pure SBA-15 is higher than the others (64.365 mJ/m^2). The

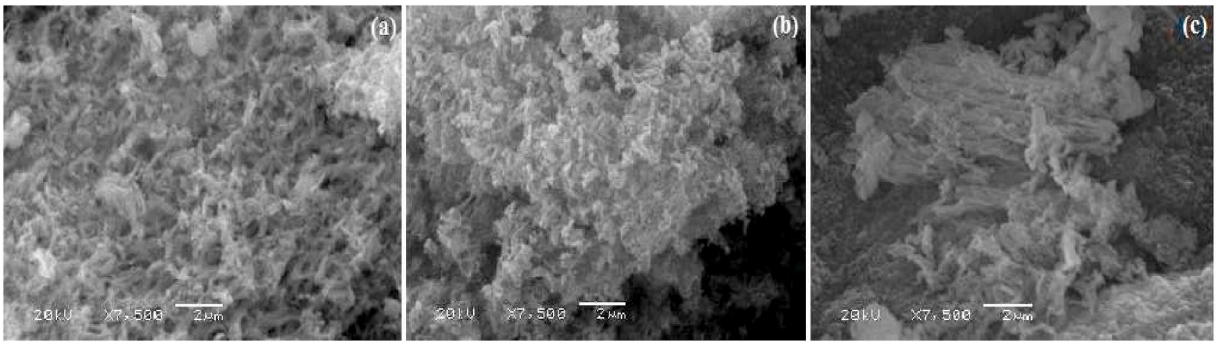

Fig. 3. SEM images of B-SBA-15-x samples (for x7500 zoom) (a) B-SBA-15-50, (b) B-SBA-15-30 and (c) B-SBA-15-10.

Table 1
Literature values of surface energy of model liquids and their components

Model liquid	γ_L (mJ/m^2)	γ_L^d (mJ/m^2)	γ_L^p (mJ/m^2)
Ethylene glycol [30]	48.0	29.0	19.0
Di-iodomethane [31]	50.8	50.8	0.00
Formamide [3]	58.0	39.0	19.0
Water [32]	72.8	21.8	51.0

Table 2
Contact angles of model liquids.

Contact Angle (°)				
	Ethylene glycol	Diiodomethane	Formamide	Water
Pure SBA-15	17.743	18.301	10.643	8.204
B-SBA-15–50	13.653	19.905	19.417	12.135
B-SBA-15–30	9.037	24.653	13.260	16.703
B-SBA-15–10	8.744	18.838	12.266	14.098

Table 3
Surface free energy values of pure SBA-15 and B-SBA-15-x samples.

Sample	γ_S (mJ/m^2)	γ_S^d (mJ/m^2)	γ_S^p (mJ/m^2)
Pure SBA-15	64.365	39.429	24.936
B-SBA-15-50	63.545	38.897	24.648
B-SBA-15-30	63.490	38.523	24.966
B-SBA-15-10	64.218	39.780	24.437

fact that the γ_S of pure SBA-15 is higher than the others is consistent with the expectation in Table 2.

In fact, as can be seen in Table 3, the γ_S, γ_S^d and γ_S^p values of all samples were found to be very close to each other. γ_S values of the samples vary between 63.4 and 64.3 mJ/m^2. After pure SBA-15, the highest surface free energy was seen with B-SBA-15-10 (64.218 mJ/m^2). γ_S^d and γ_S^p values of the samples are also very close to each other, changing between 38.5-39.8 and 24.4–25.0 mJ/m^2, respectively.

There is no study found in the literature in which the surface free energy of SBA-15 materials is determined by the contact angle technique. However, there are some results obtained by the inverse gas chromatography (IGC) technique. Therefore, the results obtained from this study were compared with results of IGC studies in the literature. For example, in Rückriem's studies, the γ_S^d value of SBA-15 was determined as 56 mJ/m^2 at 93 °C using the IGC technique [34,35]. It is known that a temperature increase decreases γ_S^d [36,37]. Our study was carried out at room temperature and the γ_S^d value of pure SBA-15 was found to be 39.43 mJ/m^2. Although the temperature was higher in Rückriem's studies, it was reported that higher γ_S^d values were found for pure SBA-15. In IGC, it is usually studied in the infinite dilution zone where very small injection quantities are applied to determine γ_S^d and a very small area of the stationary phase is examined and, that IGC evaluates the high energy regions of the stationary phase with preferential interactions of the model liquids [3,38,39]. Therefore, it can be said that the γ_S^dvalue calculated according to IGC is higher. In addition, there are studies in the literature comparing IGC and contact angle measurement (for various approaches) methods for different materials and it has been observed that the surface free energy values calculated by different methods are different from each other [3,38–40]. And in Yao's study, citing a study that stated that the results of γ_S^d obtained from the two methods could not be the same due to the difference in their theoretical approach [3]. The difference between the results obtained with IGC and contact angle methods can be explained with the above explanations. Also, since the total surface free energy (γ_S) and its polar component (γ_S^p) values are not calculated in Rückriem's studies [34,35], it may not be possible to make a clear comparison. It should also not be forgotten that there may be differences in the SBA-15 synthesis procedure and different model liquids, methods (contact angle measurement and IGC) and approaches used in the surface free energy calculations.

Looking at Table 3, it can be seen that adding boron to the structure does not have a clearly visible effect on γ_S, γ_S^d and γ_S^p values. However, it can be said that the highest (γ_S) value measured at room temperature belongs to pure SBA-15.

4. Conclusions

The following conclusions can be drawn from this investigation:

- The surface free energy components (γ_S, γ_S^d and γ_S^p) of mesoporous materials can be easily determined using the contact angle measurement technique.
- The OWRK/Fowkes approach can be used in surface free energy calculations with SBA-15 materials.
- With the materials investigated, surface free energy increases with an increase in surface polarity
- It can be concluded that there is good adhesion with good interfacial interactions, i.e. low contact angle.
- Pure SBA-15 showed the highest surface energy (γ_S) according to B-SBA-15-x samples (64.365 mJ/m2).
- Boron addition to SBA-15 materials does not have a significant effect on surface free energy values.
- Boron addition did not alter the structural properties of SBA-15 mesoporous materials.
- In addition, it is expected that some properties of the materials such as adsorption, refractory, conductivity, hardness and insulation will be developed and used in many areas of industry by using the contact angles and surface energies of the synthesized boron-containing SBA-15 materials.

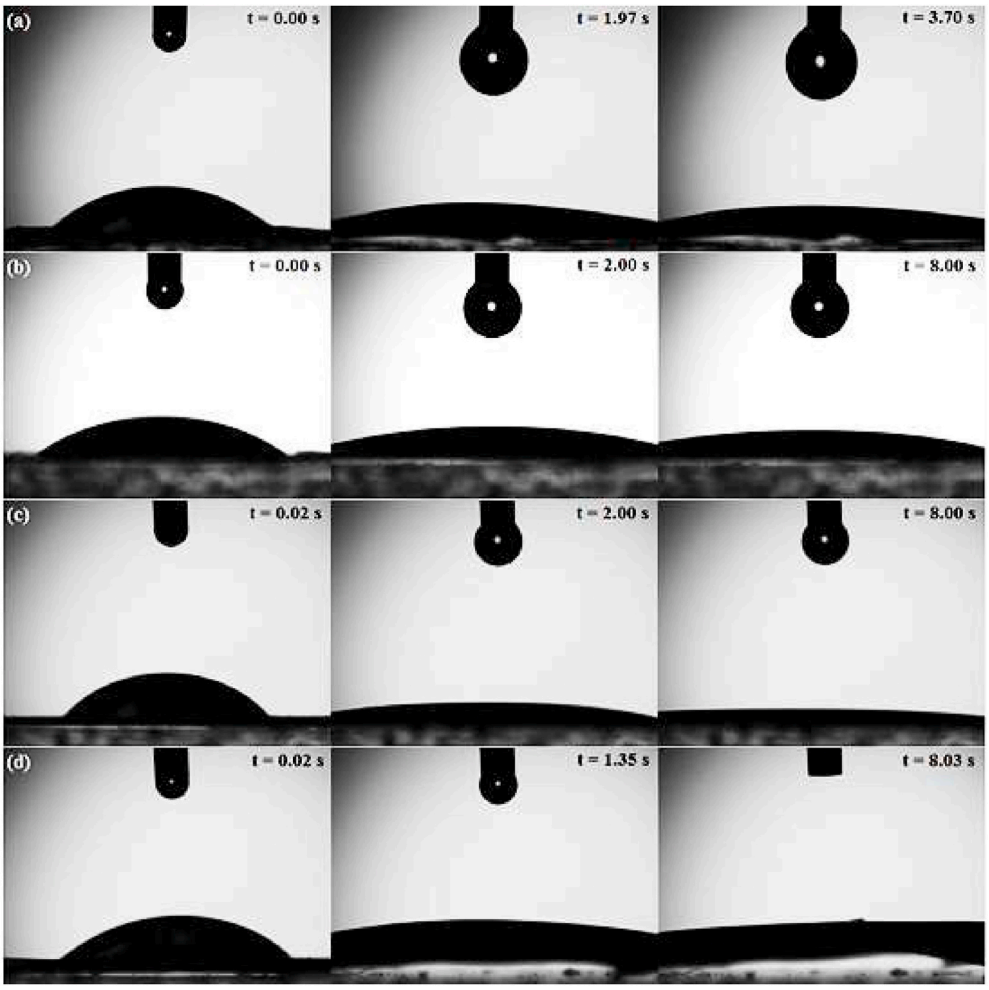

Fig. 4. Images of ethylene glycol drop placed on the sample surfaces at different stages of record (a) pure SBA-15, (b) B-SBA-15-50, (c) B-SBA-15-30 and (d) B-SBA-15-10.

Declaration of competing interest

There are no conflicts to declare.

Acknowledgements

This study was supported by Scientific Research Projects Fund of Eskisehir Osmangazi University by the project number: 2013-15049. Also, we thank Prof. Dr. Ayşegül Aşkın for a loan of the contact angle device.

References

[1] Schuster JM, Schvezov CE, Rosenberger MR. Construction and calibration of a goniometer to measure contact angles and calculate the surface free energy in solids with uncertainty analysis. Int J Adhesion Adhes 2018;87:205–15. https://doi.org/10.1016/j.ijadhadh.2018.10.012.

[2] Karde V, Ghoroi C. Influence of surface modification on wettability and surface energy characteristics of pharmaceutical excipient powders. Int J Pharm 2014;475:351–63. https://doi.org/10.1016/j.ijpharm.2014.09.002.

[3] Yao Z, Wu D, Tang J, Wu W, Heng JYY, Zhao H. A novel colored talc filler: preparation and surface property determination using two distinct methods. Chemometr Intell Lab Syst 2016;155:54–61. https://doi.org/10.1016/j.chemolab.2016.04.005.

[4] Caputo P, Miriello D, Bloise A, Baldino N, Mileti O, Ranieri GA. A comparison and correlation between bitumen adhesion evaluation test methods, boiling and contact angle tests. Int J Adhesion Adhes 2020;102:102680. https://doi.org/10.1016/j.ijadhadh.2020.102680.

[5] Rymuszka D, Terpiłowski K, Hołysz L. Influence of volume drop on surface free energy of glass. Ann UMCS, Chem 2014;68. https://doi.org/10.2478/umcschem-2013-0010.

[6] Gutiérrez A, Gomez J, Yarce CJ, Salamanca CH. Pre-formulation studies for water-dispersible powdered beverages using contact angles and wetting properties. Powder Technol 2019;353:302–10. https://doi.org/10.1016/j.powtec.2019.05.019.

[7] Salimi A, Mirabedini M, Atai M, Mohseni M. Studies of the mechanical properties and practical coating adhesion on pp modified by oxidized wax. J Adhes Sci Technol 2010;24:1113–29. https://doi.org/10.1163/016942409X12584625925105.

[8] Young III T. An essay on the cohesion of fluids. Phil Trans Roy Soc Lond 1805;95:65–87. https://doi.org/10.1098/rstl.1805.0005.

[9] Fox H, Zisman W. The spreading of liquids on low-energy surfaces. II. Modified tetrafluoroethylene polymers. J Colloid Sci 1952;7:109–21. https://doi.org/10.1016/0095-8522(52)90054-8.

[10] Fowkes FM. Determination of interfacial tensions, contact angles, and dispersion forces in surfaces by assuming additivity of intermolecular interactions in surfaces. J Phys Chem 1962;66:382–6. https://doi.org/10.1021/j100808a524.

[11] Owens DK, Wendt RC. Estimation of the surface free energy of polymers. J Appl Polym Sci 1969;13:1741–7. https://doi.org/10.1002/app.1969.070130815.

[12] Kaelble DH. Dispersion-polar surface tension properties of organic solids. J Adhes 1970;2:66–81. https://doi.org/10.1080/0021846708544582.

[13] van Oss CJ, Good RJ, Chaudhury MK. Additive and nonadditive surface tension components and the interpretation of contact angles. Langmuir 1988;4:884–91. https://doi.org/10.1021/la00082a018.

[14] Wu S. Calculation of interfacial tension in polymer systems. J Polym Sci Part C Polym Symp 1971;34:19–30. https://doi.org/10.1002/polc.5070340105.

[15] Mohamed Isa ED, Mahmud IS, Ahmad H, Abdul Rahman MB. Dependence of mesoporous silica properties on its template. Ceram Int 2019;45:12149–53. https://doi.org/10.1016/j.ceramint.2019.03.118.

[16] Todorova S, Blin JL, Naydenov A, Lebeau B, Kolev H, Gaudin P, et al. Co_3O_4-MnO_x oxides supported on SBA-15 for CO and VOCs oxidation. Catal Today 2020;357:602–12. https://doi.org/10.1016/j.cattod.2019.05.018.

[17] van Grieken R, Escola JM, Moreno J, Rodríguez R. Direct synthesis of mesoporous M-SBA-15 (M=Al, Fe, B, Cr) and application to 1-hexene oligomerization. Chem Eng J 2009;155:442–50. https://doi.org/10.1016/j.cej.2009.07.016.

[18] Selvaraj M, Kawi S. An optimal direct synthesis of CrSBA-15 mesoporous materials with enhanced hydrothermal stability. Chem Mater 2007;19:509–19. https://doi.org/10.1021/cm062009r.
[19] Moon OM, Kang B-C, Lee S-B, Boo J-H. Temperature effect on structural properties of boron oxide thin films deposited by MOCVD method. Thin Solid Films 2004; 464–465:164–9. https://doi.org/10.1016/j.tsf.2004.05.107.
[20] Siang TJ, Pham TLM, Cuong N Van, Phuong PTT, Phuc NHH, Truong QD, et al. Combined steam and CO_2 reforming of methane for syngas production over carbon-resistant boron-promoted Ni/SBA-15 catalysts. Microporous Mesoporous Mater 2018;262:122–32. https://doi.org/10.1016/j.micromeso.2017.11.028.
[21] Siang TJ, Bach LG, Singh S, Truong QD, Ho VTT, Huy Phuc NH, et al. Methane bi-reforming over boron-doped Ni/SBA-15 catalyst: longevity evaluation. Int J Hydrogen Energy 2019;44:20839–50. https://doi.org/10.1016/j.ijhydene.2018.06.123.
[22] Singh S, Nguyen TD, Siang TJ, Phuong PTT, Huy Phuc NH, Truong QD, et al. Boron-doped Ni/SBA-15 catalysts with enhanced coke resistance and catalytic performance for dry reforming of methane. J Energy Inst 2020;93:31–42. https://doi.org/10.1016/j.joei.2019.04.011.
[23] Zhao D. Triblock copolymer syntheses of mesoporous silica with periodic 50 to 300 angstrom pores. Science 1998;279:548–52. https://doi.org/10.1126/science.279.5350.548. 80-.
[24] Zhao D, Huo Q, Feng J, Chmelka BF, Stucky GD. Nonionic triblock and star diblock copolymer and oligomeric surfactant syntheses of highly ordered, hydrothermally stable, mesoporous silica structures. J Am Chem Soc 1998;120:6024–36. https://doi.org/10.1021/ja974025i.
[25] Ungureanu A, Chirieac A, Ciotonea C, Mazilu I, Catrinescu C, Petit S, et al. Enhancement of the dispersion and catalytic performances of copper in the hydrogenation of cinnamaldehyde by incorporation of aluminium into mesoporous SBA-15 silica. Appl Catal Gen 2020;598:117615. https://doi.org/10.1016/j.apcata.2020.117615.
[26] Abdullah N, Ainirazali N, Ellapan H. Structural effect of Ni/SBA-15 by Zr promoter for H_2 production via methane dry reforming. Int J Hydrogen Energy 2020. https://doi.org/10.1016/j.ijhydene.2020.07.060.
[27] Fouskas A, Kollia M, Kambolis A, Papadopoulou C, Matralis H. Boron-modified Ni/Al_2O_3 catalysts for reduced carbon deposition during dry reforming of methane. Appl Catal Gen 2014;474:125–34. https://doi.org/10.1016/j.apcata.2013.08.016.
[28] Eswaramoorthi I, Dalai AK. Synthesis, characterisation and catalytic performance of boron substituted SBA-15 molecular sieves. Microporous Mesoporous Mater 2006;93:1–11. https://doi.org/10.1016/j.micromeso.2006.01.018.
[29] Rouquerol J, Avnir D, Fairbridge CW, Everett DH, Haynes JM, Pernicone N, et al. Recommendations for the characterization of porous solids (Technical Report), 66. De Gruyter; 1994. https://doi.org/10.1351/pac199466081739.
[30] nan Li N, lu Li G, Wang H, dou, Kang J jie, Dong T shun, Wang H jun. Influence of TiO_2 content on the mechanical and tribological properties of Cr_2O_3-based coating. Mater Des 2015;88:906–14. https://doi.org/10.1016/j.matdes.2015.09.085.
[31] Gindl M, Sinn G, Gindl W, Reiterer A, Tschegg S. A comparison of different methods to calculate the surface free energy of wood using contact angle measurements. Colloids Surfaces A Physicochem Eng Asp 2001;181:279–87. https://doi.org/10.1016/S0927-7757(00)00795-0.
[32] Fowkes FM. Attractive forces at interfaces. Ind Eng Chem 1964;56:40–52. https://doi.org/10.1021/ie50660a008.
[33] Salimi A. Characterization of nano scale adhesion at solid surface of oxidized PP wax/PP blends. Int J Adhesion Adhes 2012;33:61–6. https://doi.org/10.1016/j.ijadhadh.2011.11.004.
[34] Rückriem M, Inayat A, Enke D, Gläser R, Einicke WD, Rockmann R. Inverse gas chromatography for determining the dispersive surface energy of porous silica. Colloids Surfaces A Physicochem Eng Asp 2010;357:21–6. https://doi.org/10.1016/j.colsurfa.2009.12.001.
[35] Rückriem M, Enke D, Hahn T. Inverse gas chromatography (IGC) as a tool for an energetic characterisation of porous materials. Microporous Mesoporous Mater 2015;209:99–104. https://doi.org/10.1016/j.micromeso.2014.08.053.
[36] Aşkin A, Bilgiç C. Thermodynamics of adsorption of hydrocarbons on molecular sieves NaY and CaY by inverse gas chromatography. Chem Eng J 2005;112: 159–65. https://doi.org/10.1016/j.cej.2005.04.017.
[37] Karakehya N, Bilgiç C. Inverse gas chromatographic determination of the surface energy of PMMA and PMMA/organophilic montmorillonite nanocomposites. Surf Interface Anal 2016;48:519–21. https://doi.org/10.1002/sia.5969.
[38] Papadopoulou SK, Dritsas G, Karapanagiotis I, Zuburtikudis I, Panayiotou C. Surface characterization of poly(2,2,3,3,3-pentafluoropropyl methacrylate) by inverse gas chromatography and contact angle measurements. Eur Polym J 2010; 46:202–8. https://doi.org/10.1016/j.eurpolymj.2009.11.002.
[39] Ahfat NM, Buckton G, Burrows R, Ticehurst MD. An exploration of inter-relationships between contact angle, inverse phase gas chromatography and triboelectric charging data. Eur J Pharmaceut Sci 2000;9:271–6. https://doi.org/10.1016/S0928-0987(99)00063-9.
[40] Yao Z, Wu D, Heng JYY, Lanceros-Méndez S, Hadjittofis E, Su W, et al. Comparative study of surface properties determination of colored pearl-oyster-shell-derived filler using inverse gas chromatography method and contact angle measurements. Int J Adhesion Adhes 2017;78:55–9. https://doi.org/10.1016/j.ijadhadh.2017.06.018.